CONF 910225--11

To appear in the Fourth Topical Meeting on Robotics and Remote Systems, Albuquerque, NM, February 24-28, 1991.

SAND--90-2935C

DE91 004818

DEC 1 2 1990

TECHNIQUES FOR CONTROLLING A TWO-LINK FLEXIBLE ARM

J.T. Feddema, G.R. Eisler, D.J. Segalman,
R.D. Robinett III, A.K. Morimoto, and D.A. Schoenwald
Sandia National Laboratories*
Albuquerque, N.M. 87185

Abstract

The long length and relatively small cross sectional area of the robotic arms envisioned for use inside of the underground nuclear waste storage tanks will require the control of flexible structures. This will become an important problem in the characterization and remediation of these tanks. We are developing control strategies to actively damp residual vibrations in flexible robotic arms caused by high speed motion and abrupt external forces. A planar, two-link flexible arm is currently being used to test these control strategies. In this paper, two methods of control are discussed. The first is a minimum-time control approach which utilizes a finite element model and an optimization program. These tools plan the motor torque profiles necessary for the tip of the arm to move along a straight line, in minimum time, within the motors' torque constraints, and end in a quiescent state. To account for modeling errors in the finite element model, errors in joint angles, velocities, and link curvatures are added to the optimal torque trajectory. Linear quadratic Gaussian (LQG) regulator design theory is used to determine the feedback gains. The second method of control is a teleoperated joystick controller which uses an input shaping technique to alter the commands of the joystick so as to reduce the residual vibration of the fundamental modes. Approximating the system as linear, the natural frequency and damping ratio are estimated on-line for the complete system, which includes the structure plus a lower level proportional derivative controller. An input shaping filter is determine from the estimated natural frequency, estimated damping ratio, and the desired transfer function of the system.

Introduction

The control of flexible robot manipulators may be an important issue in the waste characterization and remediation of underground storage tanks. In one possible scenario, a long slender robotic arm would be lowered through a 12 inch diameter access port and required to span the interior of a 40 feet deep by 75 feet

*Work supported by the U.S. Department of Energy at Sandia National Laboratories under Contract DE-AC0476DP00789.

MASTER

DISTRIBUTION OF THIS DOCUMENT IS UNLIMITED

diameter tank. During the waste characterization phase, the robot arm must be able to accurately position sensing instruments within the tanks while avoiding obstacles such as thermocouple trees and cooling pipes. For core sampling, the arm must come into contact with the waste surface and exert a force on a coring pipe. During the remediation stage, the robot will need to carry and accurately position waste removal equipment on or near the waste surface. Remediation techniques such as high pressure water and air jets will require that the arm be able to maintain a specified height above the surface and counteract the forces exerted by the jets. In these applications, the robot arm is expected to exhibit substantial flexible characteristics because of the relatively small cross sectional area of the arm in comparison to its length and its large payload.

While many researchers have looked at the modeling and control of a single link flexible structure, only recently has progress been made in the control of multiple flexible links. Some of the first work assumed a near perfect model of the structure existed. Bayo [1] developed a computed torque control scheme which computes the desired joint torques based on a frequency domain representation of the finite element model of the structure. Christian [2] and Singer [3] demonstrated that an input shaping method may be used to alter a joystick command so that vibration in the arm is reduced. An underdamped, second order model of the system is assumed, and the natural frequency and damping ratio of the closed loop system must first be determined from off-line measurements before the shaping filter can be applied. To compensate for modeling errors, Yurkovich and Tzes [4] developed a self-tuning controller which uses accelerometer feedback for system identification and control. Previously, we developed a feedforward control scheme [5] to perform straight line, minimum-time motions with a flexible two-link arm. An off-line, optimization program computed an optimal torque trajectory based on a finite element model of the arm, the motor torque limits, the desired tip path, and a quiescent end point position. Errors in joint angles, velocities, and link curvatures (from strain gages) were added to the optimal torque trajectory to account for modeling errors. At that time, the feedback gains were determined empirically.

This paper describes current work at Sandia National Laboratories on the control of a two-link flexible robotic arm test platform (see Figure 1). We have developed control techniques to minimize the flexible behaviors of high aspect ratio robotic arms during noncontact motions. Development continues on teleoperated as well as autonomous techniques of control.

Two methods of control are discussed in this paper. In Section 2, we provide a rigorous analysis of the feedforward controller in [5] by determining the feedback gains using linear quadratic Gaussian (LQG) regulator theory [6]. Section 3 describes a teleoperated control approach where the joystick input is modified by a filter which is based on the estimated natural frequency and damping ratio of the system and the desired response of the system. Finally, in Section 4, we summarize our results and discuss future work in this area.

DISCLAIMER

This report was prepared as an account of work sponsored by an agency of the United States Government. Neither the United States Government nor any agency thereof, nor any of their employees, makes any warranty, express or implied, or assumes any legal liability or responsibility for the accuracy, completeness, or usefulness of any information, apparatus, product, or process disclosed, or represents that its use would not infringe privately owned rights. Reference herein to any specific commercial product, process, or service by trade name, trademark, manufacturer, or otherwise does not necessarily constitute or imply its endorsement, recommendation, or favoring by the United States Government or any agency thereof. The views and opinions of authors expressed herein do not necessarily state or reflect those of the United States Government or any agency thereof.

Minimum-Time Trajectory Control

The objective of the control approach in this section is to control the tip position of the two-link flexible robot arm along a straight line between two points in minimum time subject to motor torque limits and a quiescent end point state. In this paper, a quiescent end point state will refer to having no residual vibration of the arm at the end of the desired robot motion. Before the maneuver is performed, an optimization program which utilizes a physics based finite element model of the flexible arm generates the optimal joint torque trajectories. During the maneuver, the torque trajectories are used as a feedforward term while the errors in the joint angles, velocities, and the curvature measurements (from strain gages) are used as feedback terms. A gain scheduling approach is used for the feedback terms with the gains determined off-line using a LQG regulator design. This is a viable method for highly repetitive tasks since the optimization program would only be performed once.

The finite element model of the flexible arm is an essential part of the optimization control approach. The dynamics of flexible arms can be derived in continuous time and space via Hamilton's principle; however, the resulting nonlinear integro-partial differential equations are unwieldy to deal with directly. To simplify the problem, an "assumed modes method" in which the flexure variables are expanded as a series of mode shapes can be used to reduce the dynamics to a set of nonlinear ordinary differential equations [7][8]. Others have found finite element models to be an accurate alternative approach. In this paper, a finite element model [9] is used to obtain a set of nonlinear ordinary differential equations.

In the finite element model of our two-link flexible arm, the structure was divided into 9 elements and 2 hinge joints. Figure 1 shows the Sandia two-link manipulator, and Figure 2 illustrates the geometry of the structure. The first node corresponds to the first joint or hub of the manipulator. The second node corresponds to the outer edge of the first bracket. The next three elements represent the first link divided into three equal segments with each segment having its own strain gage. The next three nodes correspond to the second bracket, second joint, and third bracket. Finally, the last three elements are the second link divided into three equal segments, again with each segment having its own strain gage. The brackets are modeled as very stiff links with large stiffness terms EI (Young's modulus times the area moment of inertia). The motion of the manipulator is assumed to take place entirely within the horizontal plane.

The dynamic equations of the finite-element model can be compactly written in the following form

$$M(\theta)\ddot{\theta} + C(\theta)\dot{\theta}^2 + K(\theta)I_1 = \bar{B}u \tag{1}$$

where θ is a column vector containing the angular positions of the 11 finite element nodes, and $u = [\tau_1 \;\; \tau_2]^T$ is the external torque vector where τ_1 and τ_2 are the applied torques at the joints. The term $\dot{\theta}^2$ is an 11x1 vector where each element is the square of $\dot{\theta}_i$. The mass matrix is $M(\theta) = [M_{i,j}cos(\theta_i - \theta_j)]$, $i = 1, \ldots, 11$, $j = 1, \ldots, 11$, the centrifugal matrix is $C(\theta) = [M_{i,j}sin(\theta_i - \theta_j)]$,

$i = 1, \ldots, 11$, $j = 1, \ldots, 11$, and the stiffness matrix is $K(\theta) = [-K_{i,j} sin(\theta_i - \theta_j)]$, $i = 1, \ldots, 11$, $j = 1, \ldots, 11$. The $M_{i,j}$ and $K_{i,j}$ in these equations are the mass and stiffness constants which are derived from the finite-element model (see [9]) and remain unchanged for a given structure (i.e., these elements do not depend on joint angles and link curvatures). The symbol I_1 refers to a column vector of 11 ones. The matrix $\bar{B}$ is an 11x2 matrix whose purpose is to transform the 2x1 control vector u into the 11x1 angular position space. It is defined as

$$\bar{B} = \begin{bmatrix} 1 & 0 & 0 & 0 & 0 & 0 & 0 & 0 & 0 & 0 & 0 \\ 0 & 0 & 0 & 0 & 0 & -1 & 1 & 0 & 0 & 0 & 0 \end{bmatrix}^T . \tag{2}$$

The reader should note that the θ_i are absolute angles in the inertial coordinate system. Because of this absolute referencing, Eq. (1) does not contain Coriolis terms ($\dot{\theta}_i \dot{\theta}_j$, $i \neq j$).

This model is efficient from a computational point of view since it only requires one evaluation of the mass and stiffness elements $M_{i,j}$ and $K_{i,j}$. It also has proven to be quite accurate in modeling the behavior of the actual manipulator. The experimental results in [5] show that the fundamental modal frequencies of the finite-element model closely approximate those of the experimental apparatus (approx. 20 Hz and 8 Hz for the first and second links respectively). In addition, the torque, angular velocity, and joint position profiles obtained by the model closely approximate those of the experimental structure for corresponding maneuvers.

The optimization problem can be formally stated as follows [10]

- minimize $J = t_f$
- with respect to the finite-element model, the actuator torque limits, and initial conditions
- subject to

$$\begin{bmatrix} x_{tip}(t_f) - x_{specified}(t_f) \\ y_{tip}(t_f) - y_{specified}(t_f) \\ \int_0^{t_f} [y_{tip}(t) - y_{specified}(t)]^2 \, dt \\ KE(t_f) \\ SE(t_f) \\ \ddot{\theta}_{joint\,1}(t_f) \\ \ddot{\theta}_{joint\,2}(t_f) \end{bmatrix} = \begin{bmatrix} 0 \\ 0 \\ 0 \\ 0 \\ 0 \\ 0 \\ 0 \end{bmatrix} . \tag{3}$$

In Eq. (3), x and y are the Cartesian coordinates of the tip of the second link or of the specified straight line trajectory, and t_f is the time it takes to complete the slew. The first two constraints assure the arm reaches the specified final tip position. The third constraint is an equality tracking constraint that keeps the tip position on the specified line. The next two constraints require the final kinetic and strain energies to be zero (i.e., final position at rest). The last two constraints force the final joint accelerations to be zero. The actuator torque limits were taken into account by limiting the torque values to 80% of the physical limits. This allowed room for additional feedback to be applied to the motors.

The optimizing program itself is a recursive quadratic programming algorithm and has been implemented on a CRAY X-MP at Sandia. It uses the aforementioned finite-element model to obtain the optimal torque profiles and the corresponding angular position and velocity values for all 11 elements at each sampling instant along the trajectory. The minimum time found by the algorithm to perform the slew in Figure 3 was 2.058 seconds. The resulting torque profile is shown in Figure 4.

Ideally, this torque profile would perform the desired motion if the experimental apparatus had the same physical parameters as the model. Unfortunately, modeling errors always exist. As shown in Figure 3, some error in the end point position was measured in our experiment when the optimal torque profile was applied without any feedback. To compensate for these modeling errors, a feedforward control scheme was implemented as shown in Figure 5. The feedback gains were determined using LQG regulator theory.

In order to apply LQG regulator theory, the dynamics in Eq. (1) must be put into state space form and then linearized about the desired trajectory. The state variables are chosen to be the 11 nodal positions and the 11 nodal velocities:

$$x_i = \theta_i \,, i = 1, \ldots, 11 \,, \quad x_{i+11} = \dot{\theta}_i \,, i = 1, \ldots, 11 \tag{4}$$

where x_i are the new state variables. Rewriting Eq. (1) in state space form,

$$\begin{bmatrix} \dot{x}_1 \\ \vdots \\ \dot{x}_{11} \\ \cdots \\ \dot{x}_{12} \\ \vdots \\ \dot{x}_{22} \end{bmatrix} = \begin{bmatrix} z_{12} \\ \vdots \\ z_{22} \\ \cdots \\ \\ M(x)^{-1}S(x) \\ \\ \end{bmatrix} + \begin{bmatrix} 0 & 0 \\ \vdots & \vdots \\ 0 & 0 \\ \cdots & \\ \\ M(x)^{-1}\bar{B} \\ \\ \end{bmatrix} u \tag{5}$$

or more compactly

$$\dot{z} = f(x) + g(x)u \,. \tag{6}$$

The matrix $M(x)$ is simply the matrix $M(\theta)$ with the θ_i's replaced with the appropriately numbered states x_i. The control vector u is as described earlier, and the matrix $S(x)$ is the matrix $S(\theta, \dot{\theta}) = -C(\theta)\dot{\theta}^2 - K(\theta)I_1$ with θ and $\dot{\theta}$ replaced by the state vector x.

The state space described in Eq. (6) is a 22nd order nonlinear ordinary differential equation. To perform the linearization about a trajectory point, we let Δx represent the perturbation in the state x about the operating point $\bar{x}$, and Δu represent the perturbation in the control input u about the operating point $\bar{u}$:

$$x = \bar{x} + \Delta x \quad \text{and} \quad u = \bar{u} + \Delta u \,. \tag{7}$$

These operating points $\bar{z}$ and $\bar{u}$ are those from the off-line optimization in Eq.(3). Truncating second and higher order terms, we obtain the following linearized model

$$\Delta\dot{x} = \left(\frac{\partial f}{\partial x} \Big|_{x=\bar{x}} + \frac{\partial g}{\partial x} \Big|_{x=\bar{x}} \bar{u} \right) \Delta x + g(\bar{x})\Delta u \quad = \quad A\Delta x + B\Delta u \tag{8}$$

where Δx represents deviations from the desired trajectory which we drive to zero.

Next, the states are transformed into a more measurable form. In our system, we have joint encoders and tachometers which measure the angular position and velocity of each joint node with respect to the previous node. We also have strain gages on the links which measure the angular position of a node with respect to the previous node. Since all position and velocity measurements of one node are relative to the previous node, it is desirable to transform the state vector by a 22x22 matrix T such that

$$\Delta z = T\Delta x \quad \text{where} \quad T_{i,j} = \begin{cases} 1 & \text{if } i = j \\ -1 & \text{if } i = j-1 = 2,3,...,11,13,14,...,22 \\ 0 & \text{otherwise} \end{cases} \tag{9}$$

Using Δz as the new state variable, Eq. (8) may be written as

$$\Delta \dot{z} = TAT^{-1}\Delta z + TB\Delta u = \tilde{A}\Delta z + \tilde{B}\Delta u\,. \tag{10}$$

The linear quadratic regulator portion of this problem is to minimize a quadratic cost criterion

$$J = \frac{1}{2}\int_0^\infty (\Delta z^T Q \Delta z + \Delta u^T R \Delta u)dt \tag{11}$$

with respect to the control vector Δu subject to the system's dynamics in Eq. (10). The choice of weighting matrices Q and R are up to the system designer. The solution to this problem involves solving an Algebraic Riccati Equation [6] for a matrix P

$$0 = \tilde{A}^T P + P\tilde{A} - P\tilde{B}R^{-1}\tilde{B}^T P + Q \tag{12}$$

which results in the feedback equation

$$\Delta u = -R^{-1}\tilde{B}^T P \Delta z\,. \tag{13}$$

Thus, the optimal *full* state feedback gain matrix is $K = -R^{-1}\tilde{B}^T P$.

Since we are unable to measure all of the states, a linear quadratic estimator design is used to determine an estimator gain matrix L which produces a linear quadratic Gaussian optimal estimate of Δz from the measurements y. The problem is formally stated as follows. Given a continuous-time system with state and measurement equations

$$\Delta \dot{z} = \tilde{A}\Delta z + \tilde{B}\Delta u + Gw \tag{14}$$

$$\Delta y = C\Delta z + v \tag{15}$$

and process and measurement noise means and covariances

$$E[w] = E[v] = 0, \quad E[ww^T] = W, \quad E[vv^T] = V\,, \tag{16}$$

the optimal state estimate $\Delta\hat{z}$ is found by integrating

$$\Delta\dot{\hat{z}} = \tilde{A}\Delta\hat{z} + +\tilde{B}\Delta u + L[\Delta y - C\Delta\hat{z}], \quad \Delta\hat{z}(0) = 0 \tag{17}$$

where

$$L = SC^T V^{-1} \tag{18}$$

and S satisfies the Algebraic Riccati Equation

$$0 = \tilde{A}S + P\tilde{A}^T - SC^T V^{-1} CS + GWG^T . \tag{19}$$

Similar to the linear quadratic gain in Eq. (13), Eq. (18) can be determined off-line and the gains scheduled for on-line control. However, at present, we do not have the on-line computing power to solve the integration in Eq. (17) in real-time; even the discrete version is computationally intensive. If the integration in Eq.(17) is approximated in discrete time as

$$\begin{aligned} \Delta\hat{z}_k \approx\ & \Delta\hat{z}_{k-1} + [\tilde{A}\Delta\hat{z}_{k-1} + \tilde{B}u_{k-1}]\Delta t \\ & + L_k\{\Delta y_k - C[\Delta\hat{z}_{k-1} + (\tilde{A}\Delta\hat{z}_{k-1} + \tilde{B}\Delta u_{k-1})\Delta t]\} \end{aligned} \tag{20}$$

we can reduce Eq. (20) to

$$\Delta\hat{z}_k \approx L_k \Delta y_k \tag{21}$$

when the sampling time Δt is small and the previous estimated state $\Delta\hat{z}_{k-1}$ reaches the desired state $\Delta z_{k-1} = 0$. Combining Eqs. (13) and (21), the approximate feedback gain at time k is $K_k L_k$.

The system software package MATLAB was used to determine the approximate feedback gain matrices $K_k L_k$ for one hundred set points along the optimal trajectory. At some points along the trajectory, the gains varied considerably. When the set of gains was used to control the system, the results were less than satisfactory. Although the arm did reach the desired end point, there was considerable error in the tip position along the way. It appeared that some of the larger scheduled gains produced unwanted effects. Again, we must remember that these gains are computed from a model of the system, so the gains are only as good as the model itself. In an attempt to reduce the sensitivity of the feedback gains to modeling errors, a single gain matrix equal to the average of the time sequence of matrices was used. Figure 3 shows the resulting tip trajectory. The averaging process removed the abrupt changes in gains along the path. Although further testing is necessary, we believe that an even better solution would be to use a set of three or four gains which would be scheduled to become active when major changes in the states occurred, e.g., when the applied torque on joint 1 changed from -6 N-m to +6 N-m.

In the LQG design, the 10x22 observation matrix C was

$$C_{i,j} = \begin{cases} 1 & \text{if } (i,j) = (1,1),(5,7) \text{ (joint angles)} \\ 1 & \text{if } (i,j) = (2,3),(3,4),(4,5),(6,9),(7,10),(8,11) \text{ (strain gages)} \\ 1 & \text{if } (i,j) = (9,12),(10,18) \text{ (joint velocities)} \\ 0 & \text{otherwise} \end{cases} \tag{22}$$

where i denotes the observation vector index and j denotes state vector index. The state and input weighting matrices were

$$Q_{i,j} = \begin{cases} 1000 & \text{if } i = j = 1,7 \text{ (joint angles)} \\ 0.1 & \text{if } i = j = 12,18 \text{ (joint velocities)} \\ 0 & \text{otherwise} \end{cases} \tag{23}$$

and

$$R = \begin{bmatrix} 1000 & 0 \\ 0 & 1000 \end{bmatrix}. \tag{24}$$

The state and measurement noise matrices were

$$W_{i,j} = \begin{cases} 0.01 & \text{if } i = j \\ 0 & \text{otherwise} \end{cases} \tag{25}$$

and

$$V = \begin{bmatrix} 0.1 & \text{if } i = j = 1,5 \text{ (joint angles)} \\ 1000 & \text{if } i = j = 2,3,4,6,7,8 \text{ (strain gages)} \\ 5 \times 10^6 & \text{if } i = j = 9,10 \text{ (joint velocities)} \\ 0 & \text{otherwise} \end{bmatrix} \tag{26}$$

In this experiment, we chose the Q matrix and the V matrix so that the majority of our feedback came from the joint encoders and tachometers. However, even with the matrices above, the gains corresponding to the strain gages were non-zero. We did this for two reasons. First, the strain gages are slightly noisier than the joint encoders and tachometers. Second, for the specified straight line slew, the tip position of the arm was dependent more on the joint positions than on the curvature of the links. We found that penalizing the link curvature states often resulted in instability because the controller put to much emphasis on the errors between the measured and modeled link curvatures. We believe that the main problem was that the linearized model was not accurate enough to properly drive the link curvature measurements to those determined by the model. With improved parameter estimation, we would be able to put more emphasis on these curvature states.

Teleoperated Control

The second method of control is an input shaping technique in which a joystick input is convolved with a filter which shapes the input so as to cancel out vibration modes. This filter is a function of the modal frequencies and damping coefficients of the system, which change with the configuration of the arm and the arm's payload. At Sandia, we are developing a technique to estimate the modal frequencies and damping coefficients and update the filter in real time. This will allow the robot to adjust to unknown payloads.

Currently, one strain gage on each link of the arm is used to measure the link's curvature as a function of time. These two measurements are used to determine the dominant mode of vibration on each link. The desired velocity of the joints as commanded by the joystick are used as the input to the system. By taking the FFT (Fast Fourier Transform) of both the output (strain gage measurements) and the input (commanded joint velocities) and dividing, the system's transfer function can be determined. The FFT of each transfer function is fit to an underdamped second order model using the Levenberg-Marquardt method [11]. The natural frequency and damping ratio determined from this nonlinear fit are then used to adjust the system's control. Figure 6 shows a block diagram of the control system. To improve robustness of the estimation process, the parameters

of the system will only be estimated when the excitation of the system is above a certain threshold.

Two methods of input shaping are currently used to adjust the joystick command being sent to a proportional-derivative joint angle controller. The first method [3] uses the natural frequency and damping ratio to determine the magnitude and spacing of three impulse functions which form the input shaping filter. The problem with this method is that the system response is delayed by the period of natural vibration. Therefore, for a typical measured frequency of natural vibration of 1 Hz, the delay is equal to one second. In many tightly constrained teleoperated situations, this delay is unacceptable.

The second method of input shaping determines the filter based on the desired transfer function of the system. Let us assume that the system is underdamped (see Figure 7) and the measured transfer function of the system is

$$H(s) = \frac{A\omega^2}{s^2 + 2\xi\omega s + \omega^2} \tag{27}$$

where A is the amplitude, ω is the natural frequency, and $0 < \xi < 1$ is the damping ratio. We would like the system to have a critically damped response and the desired transfer function to be

$$H_d(s) = \frac{A\omega_d^2}{(s + \omega_d)^2} \tag{28}$$

where ω_d is the desired natural frequency as shown in Figure 8. Assuming a linear time invariant system, we should get the desired response if the transfer function of the filter is

$$F(s) = \frac{H_d(s)}{H(s)} = \frac{\omega_d^2}{\omega^2}\frac{(s^2 + 2\xi\omega s + \omega^2)}{(s + \omega_d)^2}. \tag{29}$$

This results in the continous time domain filter

$$f(t) = \frac{\omega_d^2}{\omega^2}\left[\delta(t) + 2(\xi\omega - \omega_d)e^{-\omega_d t} + (\omega^2 - 2\xi\omega\omega_d + \omega_d^2)te^{-\omega_d t}\right] \tag{30}$$

and discrete time domain filter

$$y(k) = -a_1 y(k-1) - a_2 y(k-2) + b_0 u(k) + b_1 u(k-1) + b_2 u(k-2) \tag{31}$$

where

$$\begin{aligned}
a_1 &= -2e^{-\omega_d T} \\
a_2 &= e^{-2\omega_d T} \\
b_0 &= \left(\tfrac{\omega_d}{\omega}\right)^2 [2(\xi\omega - \omega_d)T + 1] \\
b_1 &= \left(\tfrac{\omega_d}{\omega}\right)^2 [(\omega^2 - 2\xi\omega\omega_d + \omega_d^2)T^2 - 2(\xi\omega - \omega_d)T - 2]\, e^{-\omega_d T} \\
b_2 &= \left(\tfrac{\omega_d}{\omega}\right)^2 e^{-2\omega_d T}.
\end{aligned} \tag{32}$$

By judicious choice of ω_d, the designer can specify the rise time of the system. Figure 9 shows the step response of the filter for various choices of ω_d. Note that if $\omega_d > \omega$ then the initial output of the filter (and input to the system) will be of greater magnitude than the original input. This may not be desirable if the system is already near a motor torque limit when the original step was applied. In this case, the extra initial boost provided by the filter would be clipped by the motor limits. Therefore, the trade-off of this filter is that a faster response than the impulse filter [2][3] can be achieved provided that the motors can produce the necessary torque. It is up to the designer to choose ω_d so that motor torque limits are not exceeded.

Initial experimental results of this teleoperation control approach are very encouraging. Currently, we are able to perform the above procedure in a near real-time mode that is transparent to the user. The arm is moved, input and output data are collected, the FFTs are computed, the nonlinear fit is made, and a single filter is setup for the duration of the arm's motion. Every ten milliseconds, the input and output data are transferred via a VME bus from a 68030 board performing the control to an i860 board performing the FFTs and nonlinear fit. The i860 board is capable of performing a 1024 point FFT in one millisecond. After the nonlinear fit is performed, the natural frequency and the damping ratio are transferred back to the control CPU. Our tests show that we will be able to continually perform the system identification and update the filter at better than a 10 Hz rate. This will allow the system to adaptively adjust to changes in the natural frequency caused by payload variations, kinematic changes, and external disturbances.

Conclusion

In summary, we have developed control technologies that will be useful in damping vibrations in high aspect ratio robotic manipulators. We first described an autonomous method of noncontact motions in the form of a minimum-time trajectory controller. An off-line optimization program generates a torque profile according to a finite-element model of the arm. An LQG control design procedure is used to determine feedback gains which would allow the controller to compensate for modeling errors. Our testing showed that reasonable performance was obtained with this technique even with modeling errors. Future work in this area will concentrate on performing the state estimation on-line and improving the model of the system with an off-line, least squares parameter identification scheme.

A teleoperated method of control was also discussed. The system is identified by fitting the FFT of the transfer function to a second order model. The parameters of the fit are used to determine an input shaping filter which would make the system perform according to the desired transfer function. Since the identification is performed on-line, this method of control is robust to payload variations. Future work in this area will focus on improving the on-line identification process and looking at the sensitivity of the filter to parameter errors.

References

[1] Bayo, E., Papadopoulos, P., Stubbe, J., and Serna, M., "Inverse Dynamics and Kinematics of Multi-Link Elastic Robots: An Iterative Frequency Domain Approach," *The International Journal of Robotics Research*, Vol. 6, No. 6, pp. 49-62, December 1989.

[2] Christian, A.D., "Design and Implementation of a Flexible Robot," Technical Report AI-TR 1153, MIT Artificial Intelligence Laboratory, Cambridge, MA, August 1989.

[3] Singer, N.C., "Residual Vibration Reduction in Computer Controlled Machines," Technical Report AI-TR 1030, MIT Artificial Intelligence Laboratory, Cambridge, MA, January 1989.

[4] Yurkovich, S., Tzes, A., Lee, I., Hillsley, K., "Control and System Identification of a Two-Link Flexible Manipulator," *Proceedings of the 1990 IEEE International Conference on Robotics and Automation*, pp. 1626-1631, Cincinnati, OH, May 13-19, 1990.

[5] Feddema, J.T., Eisler, G.R., and Segalman, D.J., "Integration of Sensor-Based and Model-Based Control of a Two-Link Flexible Robot Arm," *Proceedings of the IEEE International Conference on Systems Engineering*, pp. 435-439, Pittsburgh, Pennsylvania, August 9-11, 1990.

[6] Stengel, R.F., *Stochastic Optimal Control: Theory and Application*, John Wiley & Sons, New York, 1986, p. 464.

[7] Khorrami, F., "Analysis of Multi-link Flexible Manipulators via Asymptotic Expansions," *Proceedings of the 28th IEEE Conference on Decision and Control*, pp. 2089-2094, Tampa, FL, December 1989.

[8] Schoenwald, D.A., Özgüner, Ü., and Chan, H., "An Analysis of Distributed Vibration Control of Flexible Manipulators using Integral Manifolds," *Proceedings of the 28th IEEE Conference on Decision and Control*, pp. 2095-2100, Tampa, FL, December 1989.

[9] Segalman, D.J., "A Mathematical Formulation for the Rapid Simulation of a Flexible Multilink Manipulator," SAND89-2308, Sandia National Laboratories, Albuquerque, NM.

[10] Eisler, G.R., Segalman, D.J., and Robinett, R.D., "Approximate Minimum-Time Trajectories for Two-link Flexible Manipulators," *Proceedings of the 1990 American Control Conference*, San Diego, CA, May 23-25, 1990.

[11] Press, W.H., Flannery, B.P., Teukolsky, S.A., and Vetterling, W.T., *Numerical Recipes in C*, Cambridge University Press, Cambridge, 1988, pp. 540-547.

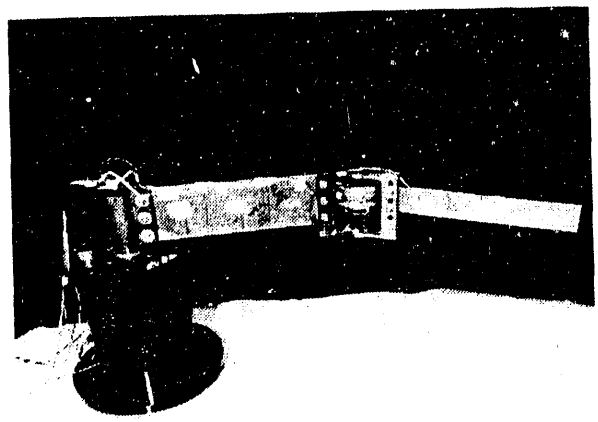

Figure 1. Sandia's two-link flexible robotic arm test platform.

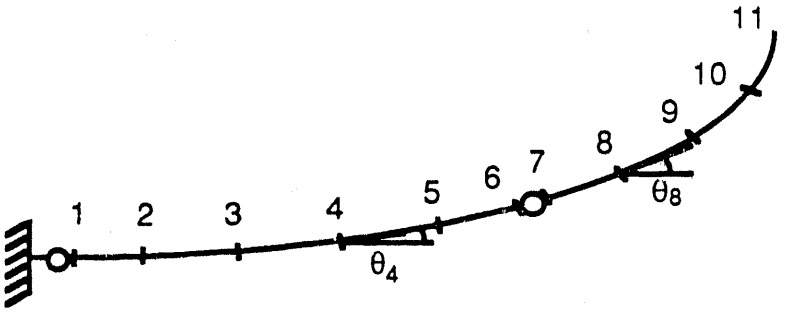

Figure 2. Geometry of finite-element model of the two-link flexible robot arm.

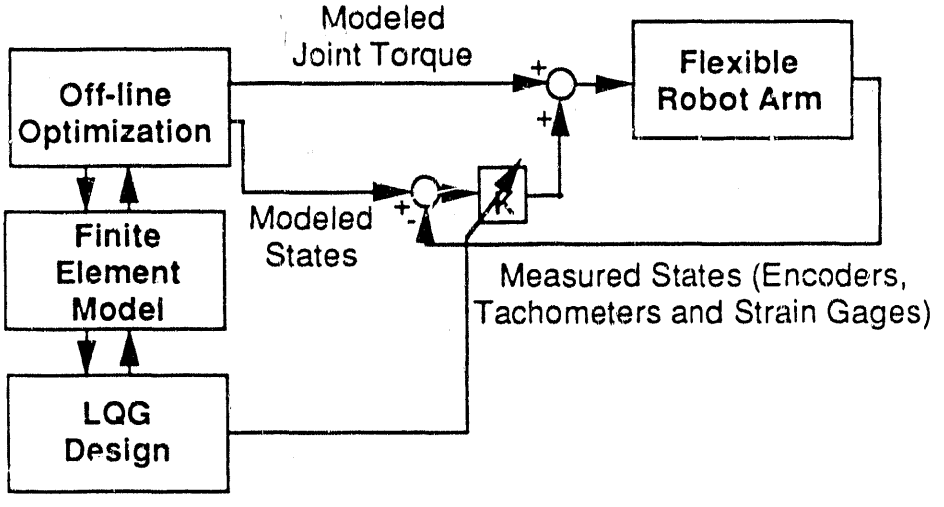

Figure 5. Feedforward Control with LQG regulator design.

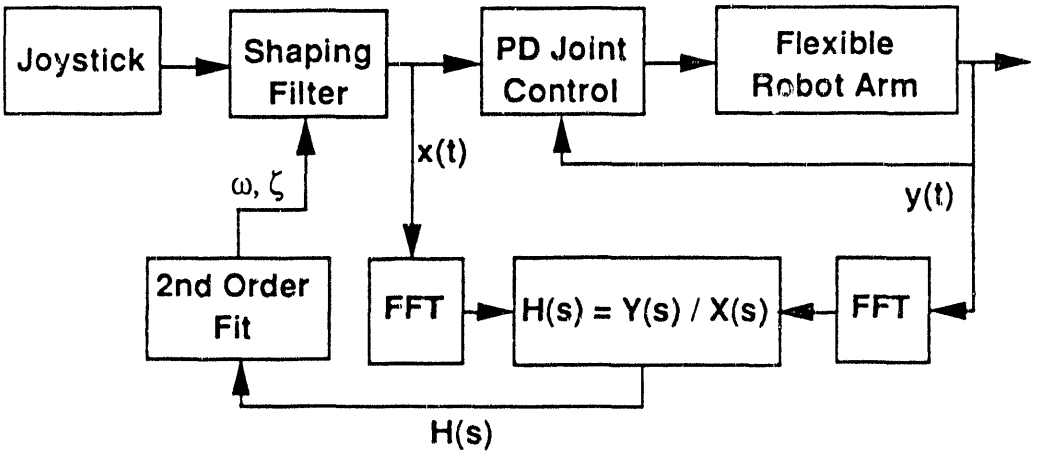

Figure 6. Input Shaping with Real-Time Parameter Identification

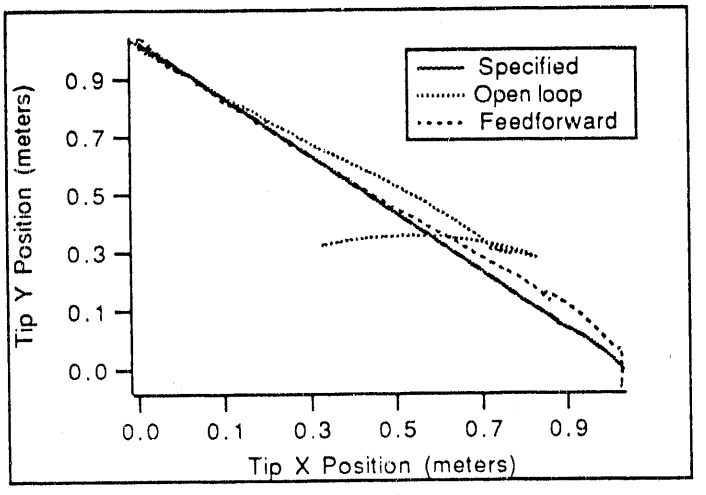

Figure 3. Specified , open loop, and feedforward control tip positions.

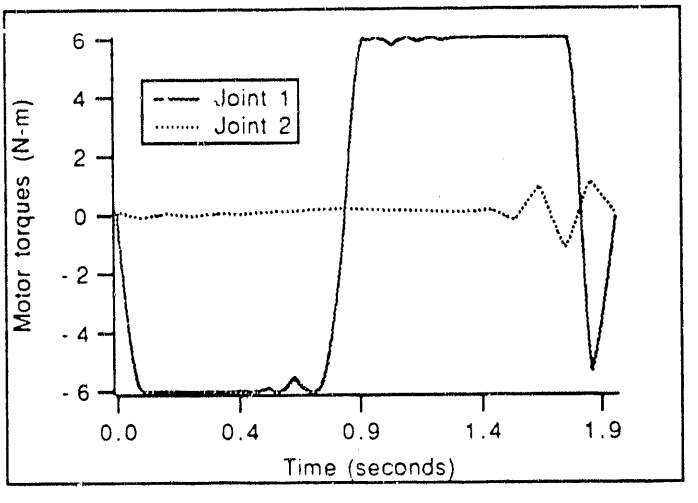

Figure 4. Motor torque profiles determined by the off-line optimization.

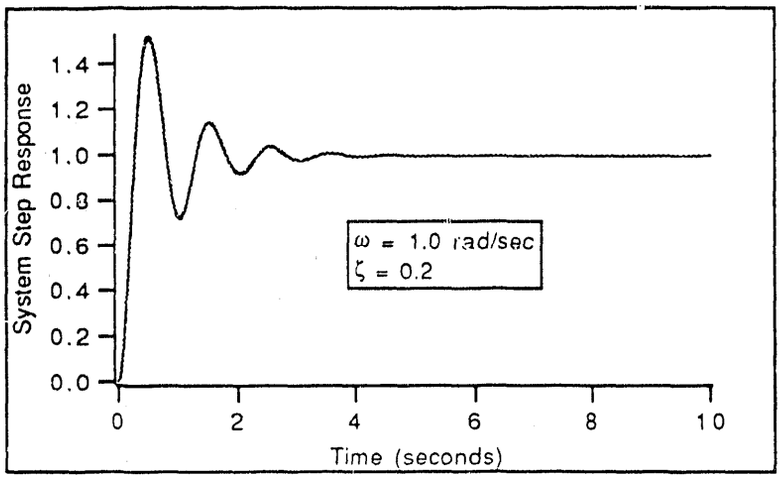

Figure 7. Underdamped second order system response of system without input shaping.

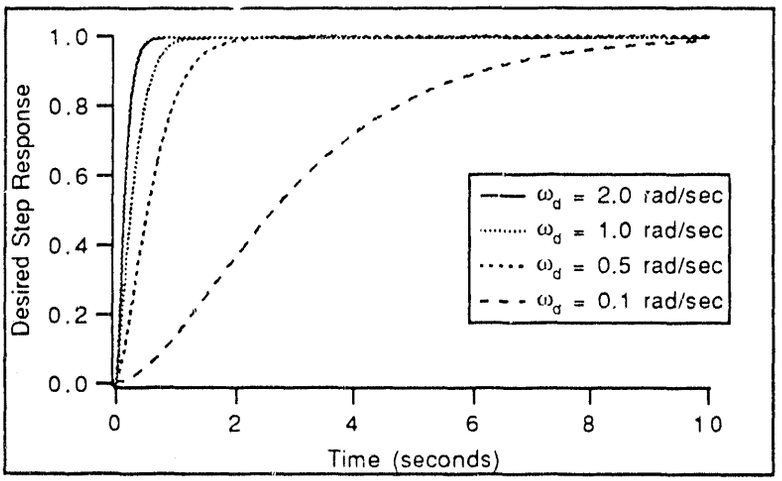

Figure 8. Desired critically damped second order response of system.

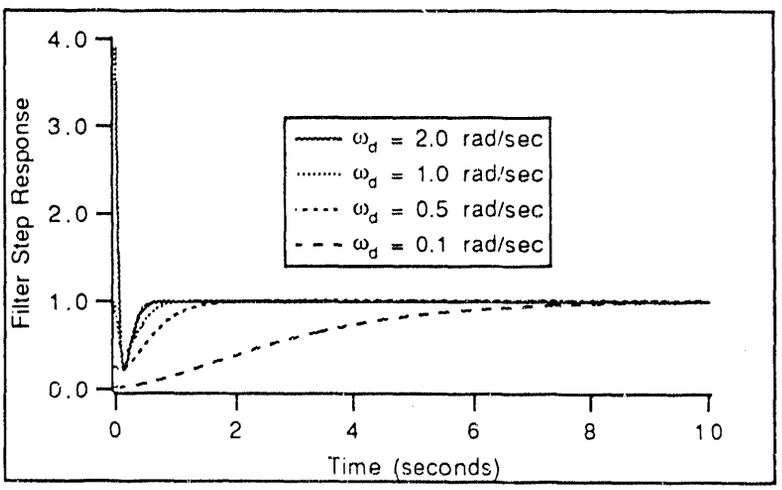

Figure 9. Input shaping filter required to achieve the desired response.

END

DATE FILMED

01 / 08 / 91